Astron. Astrophys. 359, 181–190 (2000)

ASTRONOMY AND ASTROPHYSICS

A study of Li-rich stars discovered by ROSAT in Taurus-Auriga⋆

R. Wichmann[1], **G. Torres**[2], **C.H.F. Melo**[3], **S. Frink**[4,9], **S. Allain**[5], **J. Bouvier**[5], **J. Krautter**[6], **E. Covino**[7], **and R. Neuhäuser**[8]

[1] Hamburger Sternwarte, University of Hamburg, Gojenbergsweg 112, 21029 Hamburg, Germany (rwichmann@hs.uni-hamburg.de)
[2] Center for Astrophysics, 60 Garden Street, Cambridge, MA 02138, USA
[3] Observatoire de Geneve, 51, Ch. des Maillettes, 1290 Sauverny, Suisse
[4] Astronomisches Rechen-Institut Heidelberg, Mönchhofstrasse 12–14, 69120 Heidelberg, Germany
[5] Laboratoire d'Astrophysique, Observatoire de Grenoble, B.P. 53X, 38041 Grenoble Cedex, France
[6] Landessternwarte Königstuhl, 69117 Heidelberg, Germany
[7] Osservatorio Astronomico di Capodimonte, Via Moiariello 16, 80131 Napoli, Italy
[8] Max-Planck-Institut für Extraterrestrische Physik, Giessenbachstrasse 1, 85740 Garching, Germany
[9] UC San Diego, Center for Astrophysics and Space Sciences, 9500 Gilman Drive, La Jolla, CA 92093-0424, USA

Received 21 December 1999 / Accepted 2 May 2000

Abstract. In recent years, large numbers of lithium-rich stars were discovered near several nearby star forming regions (SFRs). We present a detailed study of those stars discovered in and near the central region of the Taurus-Auriga T Tauri association, based on high-resolution echelle spectroscopy and proper motion data. We find that about 60 per cent of our sample can be regarded as pre-main sequence (PMS) stars, while the remaining stars likely are foreground zero-age main sequence (ZAMS) stars. We conclude that the PMS stars are likely associated with the Taurus-Auriga SFR, while the ZAMS stars may represent a population of somewhat older Gould Belt stars. The fraction of ZAMS stars in the Taurus-Auriga sample studied in this work is larger than in a similar sample in the Lupus SFR, and we argue that this may be explained by the spatial structure of the Gould Belt and the Sun's location within it.

Key words: stars: kinematics – stars: pre-main sequence – stars: rotation – X-rays: stars – Galaxy: open clusters and associations: individual: Golud Belt

1. Introduction

In a number of studies devoted to the follow-up observation of ROSAT All-Sky Survey (RASS) x-ray sources in the vicinity of nearby star forming regions (SFRs), large numbers of these could be identified with Li-rich stars (Wichmann et al. 1996; Alcalá et al. 1995; Alcalá et al. 1996; Neuhäuser et al. 1995; Krautter et al. 1997; Wichmann et al. 1997b; Magazzù et al. 1997). Throughout this paper, we will refer to these papers as the 'RASS-papers'. Originally these Li-rich stars were classified as weak-line T Tauri stars (WTTSs) in the RASS-papers. In this paper, we will use the more neutral designation 'ROSAT Li-rich stars' (ROSAT LRSs), as not necessarily all of them are bona-fide pre-main sequence (PMS) stars.

A number of studies carried out up to now (cf. Covino et al. 1997, Neuhäuser et al. 1997, Frink et al. 1997, and Wichmann et al. 1999), have shown that the ROSAT LRSs typically are a mixture of PMS stars and older, i.e. zero-age main sequence (ZAMS) stars. The fraction of PMS stars varies among regions, ranging from slightly above 50 per cent in Chamaeleon (Covino et al. 1997) up to some 90 per cent in Lupus (Wichmann et al. 1999).

Thus, at least a large fraction of the ROSAT LRSs represents a hitherto unknown population of PMS stars outside molecular clouds and young associations. The study of Wichmann et al. 1997b has shown that in Lupus, the ROSAT LRSs are closely correlated with the Gould Belt (Gould 1879; for a recent review of the Gould Belt see Pöppel 1997), while their surface density rapidly *decreases* towards the galactic plane. Likewise, the study of Magazzù et al. 1997 shows that in Taurus also, both far from molecular clouds and from the Gould Belt, only very few Li-rich stars are found.

While the youth of these stars makes them very interesting for studies of the evolution of stellar rotation and activity on the approach to the main sequence, their correlation with the Gould Belt presumably will allow to study the evolution and history of this structure in more detail. The Gould Belt is most prominently seen in the large number of massive stars formed at its expanding rim. Obviously, there must exist an even larger population of low-mass stars accompanying these massive stars. Moreover, as low-mass stars have much longer lifetimes, they should allow to study the full disk of the Gould Belt, contrary to the massive stars that are found primarily at its rim.

So far, it has been a problem to disentangle this presumed population of Gould Belt low-mass stars from the background of older stars within the Gould Belt (e.g. the sun). However, it has been shown that in the RASS there is a prominent enhancement of stellar x-ray sources that correlates very well with the Gould

Send offprint requests to: R. Wichmann

⋆ Based on observations obtained at Observatoire de Haute Provence. Some of the observations reported here were obtained with the Multiple Mirror Telescope, a joint facility of the Smithsonian Institution and the University of Arizona.

Belt, and can be identified with a late-type stellar population associated with the Gould Belt (Guillout et al. 1998a, 1998b). It seems quite natural to identify the ROSAT LRSs found outside SFRs - at least a large fraction of them - with this population.

In order to place these stars properly into the context of stellar evolution, and to make more definite statements on their nature and origin, it is necessary to study them in detail, and to disentangle the mixture of very young, PMS, and ZAMS stars which they comprise. In this work, we present new high-resolution and proper motion data on ROSAT LRSs in Taurus-Auriga, and use these data to evaluate their evolutionary status, and study their activity and their relation to the Gould Belt.

2. Observations and data reduction

High-resolution echelle spectra were obtained at the Observatoire de Haute Provence, using the spectrograph ELODIE at the 193 cm telescope (for a detailed description of the instrument see Baranne et al. 1996). Observations took place on 14–15 Nov 1994 (observer: P. Corporon) and on 21–27 Nov 1994 (observers: S. Allain and R. Wichmann). The run was split in two because of the unfavorable position of the moon in between.

The sample selected for these observations comprised all stars with magnitudes $m_V \leq 14$ mag from Wichmann et al. 1996. However, due to technical problems (readout failures), not for all observed stars spectra are available. As the nature of this problem is independent of the stellar magnitude, we regard the sample as statistically representative for the full original, magnitude-limited sample.

The data were reduced by C. Melo at the Observatoire de Geneve, using dedicated software developed for ELODIE. Radial and rotational velocities were determined by cross-correlation with a numerical mask.

For the determination of lithium equivalent widths, all spectra of the relevant order were averaged to find regions in the continuum unaffected by metal lines. These regions then were used to fit the continuum by a straight line. The equivalent width of the Li $\lambda 6708$ line ($W_{\rm Li}$) then was determined by fitting a gaussian curve. The derivation of $W_{\rm Li}$ was performed completely independently by two of us (C. Melo and R. Wichmann). The results, which in general were consistent within 20–40 mÅ, were averaged to produce the final $W_{\rm Li}$. The uncertainty of $W_{\rm Li}$ is due to the low S/N of the spectra (typically about 10–15).

Additional high-resolution spectroscopic observations for nearly 2/3 of the sample were obtained at the Harvard-Smithsonian Center for Astrophysics (CfA). We used nearly identical echelle spectrographs on the 1.5m Wyeth reflector at the Oak Ridge Observatory (Harvard, Massachusetts), the 1.5m Tillinghast reflector at the F. L. Whipple Observatory (Mt. Hopkins, Arizona), and on the Multiple Mirror Telescope (also Mt. Hopkins, Arizona).

The observations were obtained on a number of runs over the period 1996–1998. The instrument, setup, and reduction procedures are described in detail by Neuhäuser et al. (1997). We obtained multiple observations of most of the objects to check for binarity, with an average of about 4 exposures per star. In addition to the radial velocities, derived with standard cross-correlation techniques, we determined also effective temperatures and projected rotational velocities by comparison with a large grid of synthetic spectra based on Kurucz model atmospheres. Details on these reductions are given also by Neuhäuser et al. (1997).

The results from these spectroscopic observations at OHP and CfA are shown in Table 1.

Photometric data for our sample of ROSAT LRSs in Taurus-Auriga are partly taken from Bouvier et al. 1997. Additional data were obtained at the Calar Alto Observatory, Spain, with the 1.23 m telescope and the CCD camera. The detector was a Tektronics 1024x1024 CCD with 24 μm pixels. Observations were done during several runs, on Dec 2, 1996, Nov 4–7, 1994, Dec 16–19, 1993, and Dec 29, 1993 to Jan 2, 1994. Typically six standard star fields from the list of Landolt 1983 were observed each night to transform the instrumental system into the standard BVRI system. Data reduction was performed at Landessternwarte Heidelberg using standard IRAF/apphot routines.

Assuming a distance of 140 pc, i.e. the HIPPARCOS distance of the Taurus-Auriga clouds (Wichmann et al. 1998), we have computed masses and ages using D'Antona & Mazzitelli (1994) evolutionary tracks with Canuto & Mazzitelli (1991) convection and Alexander et al. (1991) opacities. (For details on the determination of luminosities and effective temperature, we refer to Wichmann et al. 1997a). The *absolute* masses and ages provided by these tracks might be doubtful (cf. Forestini 1994, Wuchterl 1999 for alternative tracks). However, they have been used frequently in the literature, and thus are well suited for comparison. Results from photometry are displayed in Table 2.

3. Evolutionary status

For late-type stars, the presence of lithium on the stellar surface is generally considered as a sign of youth, as lithium is strongly depleted already in ZAMS stars. It is therefore possible to distinguish between PMS and ZAMS stars by comparing the lithium abundance with that of a young ZAMS cluster like e.g. the Pleiades.

Lithium abundances can be somewhat model-dependent, thus a more robust method is to compare $W_{\rm Li}$ instead of the lithium abundances. Of course $W_{\rm Li}$ depends on the effective temperature $T_{\rm eff}$, i.e. the spectral type, therefore this comparison has to be done in a $T_{\rm eff}$–$W_{\rm Li}$ diagram.

Observationally, it has been established that even in a coeval sample like the Pleiades, there is a substantial spread in $W_{\rm Li}$ for stars of equal $T_{\rm eff}$. Thus, a second parameter seems to influence the depletion of lithium, and there are strong indications that stellar rotation may be the culprit (cf. Soderblom et al. 1993). The influence of rotation, however, is theoretically poorly understood so far, and to account for it, presumably it would be necessary to know the rotational history of the star. Due to this fact, while it is well possible to make qualitative estimates of the age of individual stars, quantitative estimates would be very uncertain.

Table 1. Results from echelle spectroscopy. We list seqence number Seq from Wichmann et al. (1996), designation, spectral type SpT (Wichmann et al. 1996), equivalent widths $W_{\rm Li}$, $\Delta\,W_{\rm Li}$ (both in mÅ), effective temperatures $T^1_{\rm eff}$ from cross-correlation and $T^2_{\rm eff}$ from SpT (in K), $V\,\sin i^1$ from CfA data and $V\,\sin i^2$ from ELODIE data, $V^1_{\rm RAD}$ from CfA data and $V^2_{\rm RAD}$ from ELODIE data, as well as the weighted mean $\langle V_{\rm RAD}\rangle$ (all in km s^{-1}). We also add a note on spectroscopic binaries (SB1=single-lined, SB2=double-lined). Stars with $\Delta\,W_{\rm Li} < 0$ are those regarded as PMS (designation in italics), where $\Delta\,W_{\rm Li}$ is the offset to the Pleiades upper limit (see Sect. 3). RX J0424.8+2643A/B: in Wichmann et al. (1996), incorrectly the (fainter) NW star is named BD+26 718, and the SE star BD+26 718B. The SE star (=BD+26 718) is RX J0424.8+2643B in SIMBAD. The two stars annotated with '(?)SB2' have recently been reobserved (once each) at the Swiss 1.2 m-telescope on La Silla by one of us (C. Melo). A preliminary analysis of the data could not confirm their SB2 nature.

Seq	Designation	SpT	$W_{\rm Li}$	$\Delta\,W_{\rm Li}$	$T^1_{\rm eff}$	$T^2_{\rm eff}$	$V\,\sin i^1$	$V\,\sin i^2$	$V^1_{\rm RAD}$	$V^2_{\rm RAD}$	$\langle V_{\rm RAD}\rangle$	Notes
1	RX J0400.5+1935	K1	258	-55	4950	4989	82	79	15.9	16.1	15.9	
2	*RX J0403.3+1725*	K3	487	154	3600	4688	110	112	-0.3	17.6	8.7	SB1
3	RX J0405.1+2632	K2	219	-102	4775	4897	22	17	6.6	7.4	7.0	
4	*RX J0405.3+2009*	K1	352	38	4975	4989	28	25	13.9	13.4	13.8	
5	*RX J0405.7+2248*	G3	248	56	6125	5715	71	67	16.9	14.1	16.4	
6	*RX J0406.7+2018*	G1	208	31	6225	5869	30	26	15.7	15.0	15.5	
7	RX J0406.8+2541	K7-M0	0		4625	3899	32	44	17.6	17.1	17.3	SB2
8	RX J0407.8+1750	K4	257	-66	5050	4592	27	24	7.0	13.1	10.0	SB1
10	*RX J0409.1+2901*	K1	413	99	5200	4989	22	23	9.8	9.5	9.7	
11	*RX J0409.2+1716*	M1	299	213		3648		73		14.7	14.7	(?)SB2
12	*RX J0409.8+2446*	M1.5	233	147		3573		7		10.9	10.9	
13	*RX J0412.8+1937*	K6	435	215		4255		12		16.8	16.8	
15	*RX J0413.0+1612*	G1	183	6	6250	5869	9	9	9.6	9.4	9.6	
18	RX J0415.3+2044	K0	270	-23	5250	5248	30	30	14.9	13.8	14.8	
19	RX J0415.8+3100	G6	168	-38		5472		31		49.8	49.8	
22	RX J0419.4+2808	G9	120	-173		5250		10		-10.7	-10.7	
23	*RX J0420.3+3123*	K4	373	49	4675	4592	8	9	12.4	13.8	13.1	
24	*RX J0420.8+3009*	K7-M0	196	110		3899		17		19.4	19.4	
27	*RX J0423.7+1537*	K2	361	40		4897		29		15.5	15.5	
29	RX J0424.8+2643B	K0	0		5500	5248	55	55	24.6	13.5	19.1	SB1
28	*RX J0424.8+2643A*	K1	410	96	5200	4989	37	14	15.7	9.9	12.8	
30	RX J0427.1+1812	G5	158	-42	6400	5554	54	48	15.2	15.0	15.2	
31	RX J0430.8+2113	G8	141	-75	6275	5309	50	43	12.5	14.9	13.1	
36	RX J0432.7+1853	K1	253	-60	4975	4989	26	25	22.2	23.4	22.5	
37	*RX J0432.8+1735*	M2	423	337		3499		11		18.6	18.6	
40	*RX J0435.9+2352*	M1.5	485	399		3573		6		16.9	16.9	
41	*RX J0437.2+3108*	K4	359	35		4592		10		15.6	15.6	
42	*RX J0437.4+1851A*	K6	277	57	4550	4255	12	15	16.0	16.1	16.0	
43	*RX J0437.4+1851B*	M0.5	538	452	4125	3724	10	11	15.2	7.0	11.1	
44	*RX J0438.2+2023*	K2	346	25		4897		16		15.7	15.7	
45	*RX J0438.2+2302*	M1	187	101		3648		8		15.7	15.7	
46	*RX J0438.4+1543*	K3	376	43		4688		10		16.2	16.2	
47	*RX J0438.6+1546*	K1	419	105	4825	4989	24	24	18.2	19.2	18.5	
48	*RX J0439.4+3332A*	K5	495	190	4500	4406	26	24	4.8	8.7	6.8	SB1
49	RX J0441.4+2715	G8	69	-147		5309		34		17.8	17.8	
50	*RX J0441.8+2658*	G7	225	13	5450	5390	24	25	14.0	14.2	14.1	
51	RX J0443.4+1546	G7	0			5390		29		0.1	0.1	
52	RX J0444.3+2017	K1	0			4989		65		20.4	20.4	
53	RX J0444.4+1952	M1	0			3648		7		31.6	31.6	
54	RX J0444.9+2717	K1	188	-125	5625	4989	89	80	18.0	16.0	17.5	
55	*RX J0445.8+1556*	G5	357	156	5325	5554	119	114	24.1	11.2	22.8	
56	RX J0446.8+2255	M1	0			3648		10		18.0	18.0	
57	RX J0447.9+2755	K0	203	-90	6300	5248	36	27	16.3	13.6	14.9	SB2
58	RX J0450.0+2230	K1	275	-38	5000	4989	59	55	15.3	16.4	15.7	
59	*RX J0451.8+1758*	M1.5	364	278		3573		17		18.2	18.2	
61	RX J0451.9+2849B	K2	0			4897		47		16.7	16.7	
62	*RX J0452.5+1730*	K4	401	77		4592		9		16.4	16.4	
63	*RX J0452.8+1621*	K6	583	363	4500	4255	41	26	13.9	16.0	15.0	(?)SB2
64	*RX J0452.9+1920*	K5	306	1	4675	4406	6	6	14.2	15.1	14.7	
66	RX J0455.1+1826	G1	0		6300	5869	87	81	15.3	11.6	14.9	

Table 1. (continued)

Seq	Designation	SpT	$W_{\rm Li}$	$\Delta\,W_{\rm Li}$	$T^1_{\rm eff}$	$T^2_{\rm eff}$	$V \sin i^1$	$V \sin i^2$	$V^1_{\rm RAD}$	$V^2_{\rm RAD}$	$\langle V_{\rm RAD}\rangle$	Notes
67	RX J0455.7+1742	K3	247	-85	4700	4688	20	19	16.1	16.4	16.2	SB2
70	*RX J0457.0+1600*	M1	304	218		3648		9		19.8	19.8	
71	*RX J0457.0+1517*	G3	199	7	5850	5715	15	15	14.5	16.0	14.9	
72	RX J0457.0+3142	K2	138	-183	5350	4897	25	27	-15.9	-9.0	-15.7	SB1
73	*RX J0457.2+1524*	K1	446	132	4925	4989	43	42	18.0	19.9	18.6	
74	*RX J0457.5+2014*	K3	434	101	4975	4688	37	33	14.5	16.4	14.8	
75	*RX J0458.7+2046*	K7	452	360	4450	4150	6	8	18.6	18.9	18.8	
76	*RX J0459.7+1430*	K4	403	79	4700	4592	16	15	22.9	19.4	21.1	

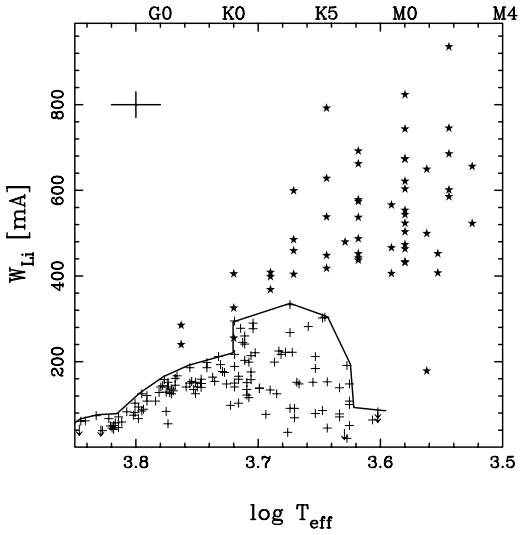

Fig. 1. $W_{\rm Li}$ vs. $T_{\rm eff}$ for Pleiades (crosses), ROSAT-discovered Taurus WTTSs (open circles), and optically discovered bona-fide TTSs (stars). Also drawn is the upper envelope for the Pleiades sample. TTS and ROSAT LRSs data have been corrected as described in the text. Typical error bars are shown upper left. On the upper border spectral types are indicated.

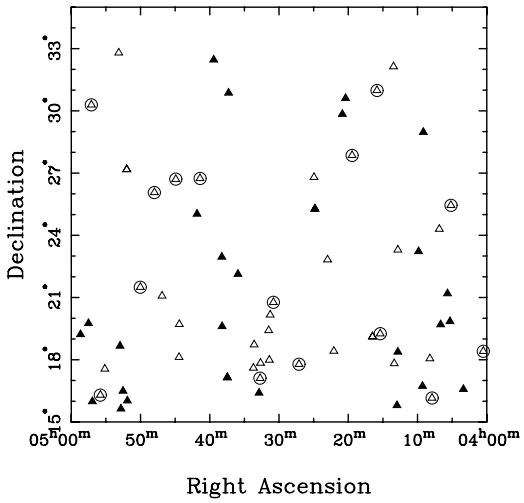

Fig. 2. Spatial distribution of observed(open triangles) and not observed (filled triangles) stars. Stars not accepted as pre-main sequence stars are encircled.

Fig. 1 shows a $T_{\rm eff}$–$W_{\rm Li}$ diagram with data for the Pleiades (Soderblom et al. 1993) and for the ROSAT LRSs in Taurus-Auriga studied by us. Also shown are optically discovered bona-fide TTSs (data from Magazzù et al. 1992; Basri et al. 1991; Martín et al. 1994). Soderblom et al. 1993 give equivalent widths corrected for the contribution of the Fe I $\lambda 6707.44$ line. For consistency, all other datapoints in the plot have been corrected for this line as prescribed by Favata et al. 1993.

Because of the spread present in the Pleiades data, we use the upper envelope of the Pleiades as the dividing line between PMS and ZAMS stars. I.e., we regard stars with a positive offset $\Delta\,W_{\rm Li}$ to the Pleiades upper envelope as PMS stars. Of course, a similar spread may be present in the ROSAT LRSs, but the upper envelope of the Pleiades appears rather well-defined. Thus, we define $\Delta\,W_{\rm Li}$ as the offset to the Pleiades upper envelope, and presume that stars with positive $\Delta\,W_{\rm Li}$ are significantly younger than the Pleiades, and may be regarded as PMS stars.

For stars with negative $\Delta\,W_{\rm Li}$, the classification is somewhat uncertain. As there is no well-defined 'Pleiades lower envelope', there seems no reason to assume the existence of a 'PMS lower envelope'. One might speculate that even stars with negative $\Delta\,W_{\rm Li}$ can be rather young. However, we regard such stars conservatively as ZAMS stars. Stars for which no lithium could be detected ($W_{\rm Li} = 0$ in Table 1) may be old main-sequence stars.

In Fig. 2 we show the distribution of observed and not observed stars from the sample of Wichmann et al. 1996. For the observed stars, those that are not classified as PMS stars are marked. As observed stars were selected by a magnitude criterion, we would not expect a strong bias with respect to their location, and in fact Fig. 2 suggests that the observed stars represent a fair sample of the total population. Also, we see no tendency of Li-poor or Li-rich stars to cluster in distinct areas. In Fig. 3 we show the HR diagram for those stars regarded as PMS.

4. 3D space motions

We calculated space velocities for all the 36 stars in Table 1 for which proper motions are available in any of the following proper motion catalogues: Hipparcos (ESA 1997), PPM (Röser & Bastian 1991), ACT (Urban et al. 1997), TRC (Høg et al. 1998) and STARNET (Röser 1996). PPM and STARNET proper motions, which are given in the original catalogues in the FK5 system, were transformed to the ICRS astrometric system de-

Table 2. Results from photometry. We list seqence number Seq from Wichmann et al. (1996), designation, spectral type SpT (Wichmann et al. 1996), V magnitude, B-V, V-R, and R-I. Luminosities and radii are computed for an assumed distance of 140 pc. Masses and ages are from comparison with evolutionary tracks from D'Antona & Mazzitelli 1994 (CM convection, Alexander opacities). RX J0435.9+2352 and RX J0441.4+2715 would fall above the birthline and below the ZAMS, respectively, for the assumed distance. Designation in italics indicates stars regarded as PMS.

Seq	Designation	SpT	V	B-V	V-R	R-I	$\log(L/L_\odot)$	$R/R_\odot$	$M/M_\odot$	$\log(age/yrs)$
1	RXJ0400.5+1935	K1	10.21	0.94	0.56	0.53	0.33	1.96	1.43	6.37
2	*RXJ0403.3+1725*	K3	11.69	1.07	0.66	0.60	-0.19	1.23	1.07	6.87
3	RXJ0405.1+2632	K2	11.47	0.82	0.50	0.43	-0.34	0.94	0.93	7.31
4	*RXJ0405.3+2009*	K1	10.38	0.88	0.53	0.49	0.19	1.67	1.37	6.57
5	*RXJ0405.7+2248*	G3	9.33	0.61	0.35	0.37	0.50	1.82	1.44	6.95
6	*RXJ0406.7+2018*	G1	9.52	0.60	0.35	0.31	0.40	1.53	1.26	7.15
7	RXJ0406.8+2541	K7-M0	11.71	1.34	0.85	0.87	0.00	0.00	0.00	0.00
8	RXJ0407.8+1750	K4	11.38	0.83	0.52	0.53	-0.27	1.15	1.01	6.93
10	*RXJ0409.1+2901*	K1	10.65	0.85	0.54	0.51	0.11	1.53	1.32	6.69
11	*RXJ0409.2+1716*	M1	13.20	1.38	0.95	1.07	-0.58	1.29	0.40	6.25
12	*RXJ0409.8+2446*	M1.5	13.30	1.42	0.97	1.08	-0.63	1.26	0.35	6.21
13	*RXJ0412.8+1937*	K6	12.51	1.25	0.80	0.83	-0.31	1.29	0.81	6.61
18	RXJ0415.3+2044	K0	10.56	0.73	0.44	0.44	0.02	1.24	1.18	7.05
19	RXJ0415.8+3100	G6	12.36	0.89	0.53	0.57	-0.38	0.72	0.90	7.95
23	*RXJ0420.3+3123*	K4	12.48	1.06	0.64	0.63	-0.55	0.84	0.83	7.41
19	*RXJ0423.7+1537*	K2	11.29	0.95	0.55	0.53	-0.15	1.17	1.11	6.99
28	*RXJ0424.8+2643A*	K1	11.31	1.31			0.32	1.93	1.42	6.39
31	RXJ0430.8+2113	G8	10.26	0.65	0.46	0.42	0.19	1.48	1.35	6.89
36	RXJ0432.7+1853	K1	10.79	0.84			-0.03	1.30	1.21	6.89
40	*RXJ0435.9+2352*	M1.5	13.57	1.44	1.18	1.29	-0.31	1.83		
41	*RXJ0437.2+3108*	K4	13.24	1.30	0.79	0.86	-0.47	0.93	0.89	7.27
44	*RXJ0438.2+2023*	K2	12.22	1.11	0.64	0.65	-0.31	0.98	0.96	7.25
45	*RXJ0438.2+2302*	M1	13.73	1.39	1.01	0.96	-0.84	0.95	0.42	6.69
46	*RXJ0438.4+1543*	K3	13.29	1.18	0.72	0.69	-0.67	0.70	0.74	7.69
47	*RXJ0438.6+1546*	K1	10.72	0.93	0.61	0.51	0.16	1.60	1.35	6.63
49	RXJ0441.4+2715	G8	13.11	0.94	0.60	0.60	-0.62	0.58		
50	*RXJ0441.8+2658*	G7	9.53	0.61	0.40	0.34	0.39	1.79	1.57	6.73
51	RXJ0443.4+1546	G7	12.84	1.04	0.60	0.66	0.00	0.00	0.00	0.00
52	RXJ0444.3+2017	K1	12.65	1.05	0.66	0.68	0.00	0.00	0.00	0.00
53	RXJ0444.4+1952	M1	12.55	1.39	0.92	1.00	0.00	0.00	0.00	0.00
54	RXJ0444.9+2717	K1	9.62	0.84	0.53	0.51	0.51	2.42	1.45	6.09
55	*RXJ0445.8+1556*	G5	9.26	0.75	0.55	0.35	0.68	2.36	1.86	6.61
71	*RXJ0457.0+1517*	G3	10.29	0.65			0.13	1.19	1.10	7.29
72	RXJ0457.0+3142	K2	10.72	1.62			0.89	3.86	1.36	5.53
73	*RXJ0457.2+1524*	K1	10.30	0.95			0.27	1.83	1.41	6.45
75	*RXJ0458.7+2046*	K7	11.91	1.24			-0.33	1.32	0.71	6.49

fined by Hipparcos. All the stars present in ACT had also proper motions in TRC, and so we used the latter one because TRC is based on a more rigorous reduction than ACT.

For stars which were still present in more than one of the catalogues the most accurate proper motion was adopted, except in the following case: if the proper motions in different catalogues were discordant, priority was given to TRC and STARNET since such large discrepancies are often due to orbital motions of double stars (Wielen 1997), so that their effect is minimized by using data with a longer baseline. In our final sample there are 2 proper motions from Hipparcos, 12 from TRC and 22 from STARNET, and the data is given in Table 4.

For the calculation of the space velocities we used the average of the radial velocities from CfA and ELODIE (see Table 1), and adopted a distance of 140 pc, corresponding to the HIPPARCOS distance of the Taurus-Auriga clouds (Wichmann et al. 1998). The space velocities have been corrected for the motion of the Sun and for differential galactic rotation (although the effect of the latter is small, typically below 0.5 km s^{-1}). The resulting histograms are shown in Fig. 4, together with the space velocities of classical and weak-line TTS known before ROSAT. Some of these data were already published and discussed in Frink et al. (1997) and Neuhäuser & Brandner (1998).

No significant differences between both samples are visible, with the exception of maybe a slight difference in the mean U velocities (see Table 3). However, note the excellent agreement between the dispersions for both samples in all the directions. The dispersion in the U velocities however is obviously smaller

Table 3. Mean and dispersion of the space velocities shown in Fig. 3. RXJ 0403.4+1725 and RXJ 0457.1+3142, which are not considered to be kinematic members, have been removed from the sample before computing the mean values. The results are quite similar for both samples.

	#	$\langle U \rangle$ [km s^{-1}]	σ_U	$\langle V \rangle$ [km s^{-1}]	σ_V	$\langle W \rangle$ [km s^{-1}]	σ_W
ROSAT WTTS (this paper)	34	-4.7	3.3	-1.8	8.2	-4.0	4.0
TTS known before ROSAT	31	-7.6	2.7	-0.7	8.6	-4.1	4.4

than the dispersion in the V or W velocities, which is a consequence of the assumption of a mean distance instead of individual distances for each star (Frink et al. 1997). The U velocities are not affected, since the direction of U roughly coincides with the direction of the radial velocities.

At least two stars can not be regarded as kinematic members of the association. RXJ 0403.4+1725 has a very high proper motion resulting in a space velocity quite different from the mean in all 3 components. However, the star has a very large $W_{\rm Li}$. It is possible that the proper motion is spurious due to a misidentification of the star on the plates (Frink et al. 1997). Another explanation would be that the star is a run-away TTS ejected by gravitational few-body interaction, a mechanism discussed by Sterzik & Durisen (1998). Similarly, the radial velocity of RXJ 0457.1+3142 is rather conspicuous and inconsistent with kinematic membership to Taurus, which is in line with its low $W_{\rm Li}$. However we caution that RXJ 0457.1+3142 is a binary, and the radial velocity thus is approximate only.

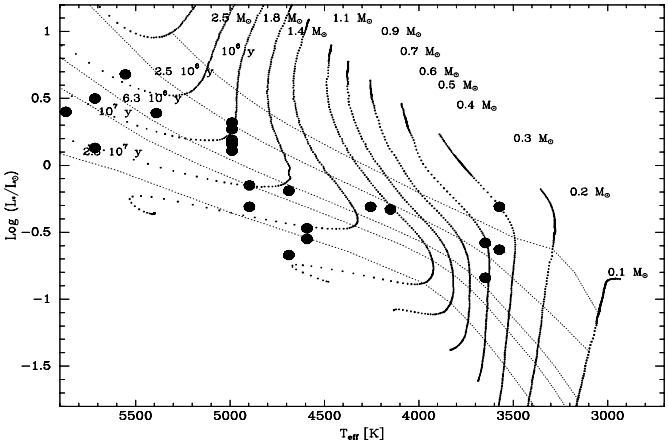

Fig. 3. HR diagram for stars regarded as pre-main sequence. Evolutionary tracks are from D'Antona & Mazzitelli (1994), with Canuto & Mazzitelli (1991) convection and Alexander et al. (1991) opacities.

5. Mean distance

Given the rotational period $\rm P_{rot}$ as well as $\rm V \sin \it i$ and $\sin i$, it is possible to compute the stellar radius R as

$$R = \frac{P_{\rm rot} V \sin i}{2\pi \sin i}.$$

With photometric data available, the distance r of the star then might be estimated as

$$\rm r = \sqrt{\frac{R^2 \pi B_{\nu,T_{eff}}}{C_{\nu,T_{eff}} f_\nu}}.$$

Here, $B_{\nu,T_{\rm eff}}$ denotes the flux of a blackbody of temperature $T_{\rm eff}$ at the frequency ν, f_ν the observed flux from the star, and $T_{\rm eff}$ the effective temperature of the star (as inferred from the spectral type). $C_{\nu,T_{\rm eff}}$ is a correction factor of order unity obtained from model spectra (Hauschildt et al. 1998), to account for deviation of the stellar flux from the blackbody law.

For several stars of our sample, $P_{\rm rot}$ has been measured by Bouvier et al. (1997). As individual inclination angles are unknown, we set $\sin i$ to its mean value of $\pi/4$ (for an isotropic distribution of inclination angles), and evaluate the mean distance for the whole sample. The resulting distance is $\rm r \simeq 180 \pm 25$ pc (for stars with $\Delta\, \rm W_{Li} > 0$).

However, as already discussed by Wichmann et al. (1999), where this method is applied to ROSAT LRSs in Lupus, period detection may introduce a bias towards stars with high inclination angle. Wichmann et al. (1999) estimated that this could lead to an overestimate of the mean distance by some 13 per cent (the effect is not very high, as high inclinations are more frequent than low inclinations even for an isotropic distribution). This estimate was based on the fraction of period non-detections in the Wichmann et al. (1999) sample. A similar estimate for the Bouvier et al. (1997) sample would not be very meaningful, as many non-detections in this sample presumably are due to bad weather during the observing runs of this study. Thus, we adopt the bias estimate by Wichmann et al. (1999). This would lead to a mean distance in the range 130–180 pc for the stars of our sample.

Fig. 5 shows a histogram of the distribution of individual distances (which are, of course, subject to large errors due to the unknown inclination). As one can see, the computed mean distance might be somewhat biased by two outliers at about 300 pc.

A different method to get an idea about the distances, in the absence of direct distance determinations, is to look at the offset from the ZAMS that one obtains for some fixed distance estimate, or equivalently (as isochrones are more or less parallel to the ZAMS), at the distribution of ages one obtains.

Fig. 6 shows a box-plot of the age distributions for the stars in our sample, both for stars classified as PMS and as ZAMS. Ages (and masses), as listed in Table 2, were estimated using the evolutionary tracks from D'Antona & Mazzitelli (1994). Following Wichmann et al. (1997a), extinctions were estimated from the $V - I_C$ colours, bolometric luminosities were computed from the dereddened R_C magnitudes, and effective tem-

Table 4. Positions and proper motions for all the 36 stars for which proper motions are available. In the second column, HIP stands for Hipparcos, T for TRC and S for STARNET. For the two Hipparcos stars, the parallaxes converted to distances are given in the last column.

object	cat. No.	RA ($\alpha_{J2000.0}$)	DEC ($\delta_{J2000.0}$)	m_V [mag]	μ_α [mas/a]	μ_δ	$\sigma_{\mu_\alpha \cos\delta}$ [mas/a]	σ_{μ_δ}	d [pc]
RXJ 0400.5+1935	T 1258 894	$4^h\ 0^m 31.^s07$	$+19^o35'20.''8$	10.51	6.0	-14.0	1.6	1.6	
RXJ 0403.4+1725	S 1254 309	4 3 24.86	+17 24 26. 2	11.47	-61.	-16.	3.6	3.3	
RXJ 0405.2+2632	S 1822 1383	4 5 12.34	+26 32 43. 6	11.22	18.	-25.	4.0	4.0	
RXJ 0405.3+2009	S 1258 338	4 5 19.61	+20 9 25. 2	10.20	10.	-19.	3.6	3.6	
RXJ 0405.7+2248	T 1814 409	4 5 40.58	+22 48 12. 0	9.44	2.4	-15.4	1.9	1.7	
RXJ 0406.7+2018	HIP 19176	4 6 38.80	+20 18 11. 2	10.36	6.40	-15.40	1.65	1.24	156^{+62}_{-35}
RXJ 0406.8+2541	S 1818 144	4 6 51.34	+25 41 28. 4	11.30	10.	-22.	4.2	4.2	
RXJ 0407.9+1750	S 1254 785	4 7 54.00	+17 50 26. 0	11.16	21.	-49.	3.9	3.9	
RXJ 0409.2+2901	T 1826 877	4 9 9.74	+29 1 30. 3	10.94	22.1	-27.3	2.6	3.0	
RXJ 0413.0+1612	S 1251 201	4 12 59.87	+16 11 47. 8	10.74	11.	-44.	3.8	3.8	
RXJ 0415.4+2044	T 1263 1027	4 15 22.92	+20 44 16. 9	10.50	1.8	-17.0	1.6	3.5	
RXJ 0420.4+3123	S 2371 740	4 20 24.13	+31 23 23. 6	12.18	2.	-17.	7.9	7.9	
RXJ 0423.7+1537	S 1264 822	4 23 41.36	+15 37 55. 2	10.91	12.	-10.	5.1	5.1	
RXJ 0424.8+2643A	S 1824 592	4 24 48.18	+26 43 16. 0	11.46	13.	-24.	5.0	5.0	
RXJ 0424.8+2643B	S 1824 183	4 24 49.09	+26 43 9. 4	10.47	11.	-31.	5.0	5.0	
RXJ 0427.1+1812	T 1269 1245	4 27 4.86	+18 12 27. 2	6.93	2.8	-12.4	2.2	3.2	
RXJ 0430.8+2113	T 1277 574	4 30 49.19	+21 14 10. 7	10.39	30.4	-27.3	1.9	2.1	
RXJ 0432.7+1853	T 1274 1501	4 32 42.43	+18 55 10. 2	10.83	-3.1	-11.9	1.6	1.6	
RXJ 0437.5+1851A	S 1274 1515	4 37 26.87	+18 51 25. 2	10.73	18.	-53.	3.4	3.4	
RXJ 0438.7+1546	S 1266 1195	4 38 39.02	+15 46 13. 0	9.86	0.	-30.	5.2	5.2	
RXJ 0439.4+3332A	S 2378 1232	4 39 25.47	+33 32 44. 8	11.17	28.	-42.	9.2	9.2	
RXJ 0441.8+2658	HIP 21852	4 41 55.16	+26 58 49. 4	10.34	-0.79	-20.56	1.35	1.04	115^{+21}_{-15}
RXJ 0444.9+2717	S 1839 643	4 44 54.40	+27 17 45. 5	9.00	-2.	-17.	5.1	5.1	
RXJ 0445.8+1556	T 1267 425	4 45 51.30	+15 55 49. 7	9.39	12.5	-19.6	1.7	1.9	
RXJ 0448.0+2755	S 1839 1278	4 48 0.42	+27 56 19. 8	12.35	-9.	-5.	6.3	6.3	
RXJ 0450.0+2230	S 1292 639	4 50 0.18	+22 29 57. 7	11.07	-1.	-17.	3.3	3.3	
RXJ 0452.8+1621	S 1280 559	4 52 50.15	+16 22 9. 3	11.31	7.	-17.	4.8	4.8	
RXJ 0453.0+1920	S 1288 790	4 52 57.07	+19 19 50. 1	12.07	-2.	-23.	3.9	3.9	
RXJ 0455.2+1826	T 1284 1193	4 55 9.62	+18 26 31. 1	9.26	0.4	-16.8	2.2	1.6	
RXJ 0455.8+1742	S 1284 522	4 55 47.65	+17 42 1. 9	11.16	-6.	-22.	3.9	3.9	
RXJ 0457.0+1517	T 1281 1215	4 57 0.65	+15 17 53. 1	10.53	1.2	-18.2	2.0	2.7	
RXJ 0457.1+3142	T 2388 857	4 57 6.50	+31 42 50. 5	10.90	-9.5	-10.9	2.3	2.3	
RXJ 0457.2+1524	T 1281 1288	4 57 17.66	+15 25 9. 5	10.53	10.7	-19.9	1.7	2.7	
RXJ 0457.5+2014	S 1289 513	4 57 30.63	+20 14 28. 6	10.89	-7.	-31.	3.6	3.6	
RXJ 0458.7+2046	S 1293 2396	4 58 39.71	+20 46 43. 3	11.65	0.	-35.	5.7	5.7	
RXJ 0459.8+1430	S 697 960	4 59 46.14	+14 30 55. 2	11.81	6.	-19.	5.0	5.0	

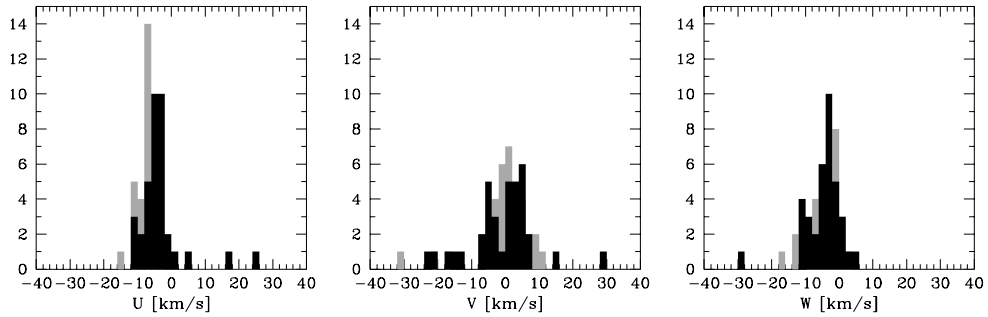

Fig. 4. Space velocity histograms for all the 36 stars in Table 4 for which proper motions are available (black) as well for the TTS known in the central Taurus region before ROSAT (grey). The velocities have been corrected for solar reflex motion and differential galactic rotation. U points in the direction of the galactic centre, V in the direction of galactic rotation and W to the northern galactic pole. No significant differences between both distributions are visible.

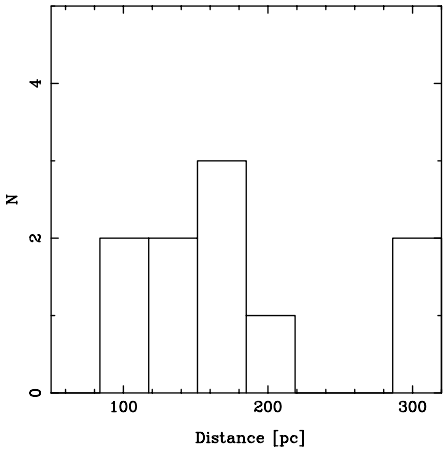

Fig. 5. Distribution of distances computed for mean value of $\pi/4$ for $\sin i$.

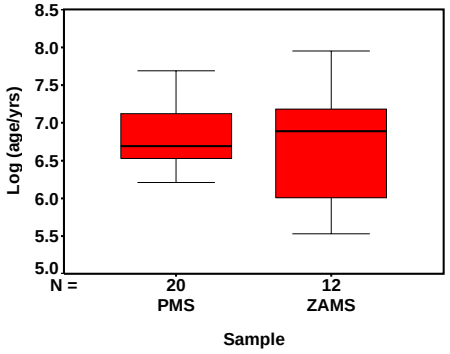

Fig. 6. Box-plot of ages estimated for an assumed distance of 140 pc, both for stars classified as PMS and as ZAMS. (The boxes mark the range between the upper and lower quartile, while the whiskers extend to the smallest and largest values less distant from the quartile points than one interquartile distance. The bold line within the box is the group median.)

peratures were estimated from spectral types (for details see Wichmann et al. 1997a). A distance of 140 pc was assumed to compute bolometric luminosities from apparent magnitudes. (In a few cases, where only B and V were measured, extinctions are from the $B-V$ colours and bolometric luminosities from the dereddened V magnitudes.)

While the PMS sample should exhibit young ages, possibly with some intrinsic spread, the ZAMS stars should show a narrow distribution near the ZAMS age, *if their distances were correctly estimated*. From Fig. 6 we can infer that their distances are, on average, overestimated. The median age estimate of $\log(age/yrs) \simeq 7$ for an assumed distance of 140 pc is equivalent to an offset of some 0.4 dex with respect to the ZAMS, thus their true mean distance should be some 60 per cent lower to place them on the ZAMS.

We also note a significantly larger spread in ages for the ZAMS sample with respect to the PMS sample. As we would expect a rather narrow spread for correct distances, given that these stars should be on the ZAMS, this large spread in estimated ages is an indication that this sample shows a correspondingly large spread in true distances, significantly larger than those stars classified as PMS.

We therefore conclude that the stars classified as PMS are consistent with a rather narrow distance distribution at a mean distance similar to that of the Taurus-Auriga SFR, while those stars classified as ZAMS show evidence of a more widespread distance distribution with typically lower values.

6. Rotation and activity

It is generally believed that the activity of late-type stars, e.g. x-ray emission, is related to magnetic fields generated by a dynamo process, and thus should correlate somehow with stellar rotation. There is in fact strong evidence for such a correlation (cf. Bouvier 1990, Simon 1990, Stauffer et al. 1994).

The use of projected rotational velocities, as obtained by our observations, in the study of this correlation has two disadvantages. As one measures $V \sin i = 2\pi R_* \sin i/P$ rather than the angular velocity $\Omega = 2\pi/P$ (where P is the rotation period), on which the dynamo effect depends (cf. Hempelmann et al. 1995), the results are subject to uncertainties both due to the unknown projection factor $\sin i$, and due to the influence of the stellar radius R_*.

In order to compare our stars with other young late-type stars, we have made use of the Open Cluster Database[1] to collect a large sample of young stars for which rotational velocities are available. We used data for stars in α Per, Hyades, IC 2602, IC 2391, IC 4665, Pleiades, and Preasepe. X-ray data were collected from Prosser et al. (1996), Stern et al. (1995), Randich et al. (1995), Giampapa et al. (1998), Stauffer et al. (1994), and Randich & Schmitt (1995). To reduce the influence of stellar radii, we divided $V \sin i$ by R_* to obtain $\Omega \sin i$. For our sample, we use R_* from Table 2, while for the open cluster stars, we computed the radii from $M_{\rm bol}$ and $T_{\rm eff}$ under the assumption of blackbody radiation.

In Fig. 7 we show, side by side, $\log(L_x/L_{bol})$ vs. $V \sin i$ (left) and vs. $\Omega \sin i$ (right). The latter plot shows a notable improvement in the tightness of the correlation of stellar activity and rotation. Also, only in the right plot it becomes obvious that one of the stars (HE 577) is a very significant outlier. This has already been noted by Randich et al. (1996). The membership of the star to the α Per cluster is doubtful (Prosser 1992).

As one can see from Fig. 7, the stars of our Taurus sample populate the same area of the diagrams as other active late-type stars. However, there are no ultra-fast rotators (like in the 'young' ZAMS clusters) in our sample. This may be just an effect of the smaller sample size – even in the 'young' ZAMS clusters like α Per, only a small fraction of the stars are actually ultra-fast rotators.

The lower part of the diagram ($\log(L_x/L_{bol}) < -4.0$) is almost exclusively populated by stars of the Hyades and the

[1] Open Cluster Database, as provided by C.F. Prosser (deceased) and J.R. Stauffer, and which currently may be accessed at http://www-cfa.harvard.edu/~stauffer/, or by anonymous ftp to cfa-ftp.harvard.edu (131.142.25.222), cd /pub/stauffer/clusters/.

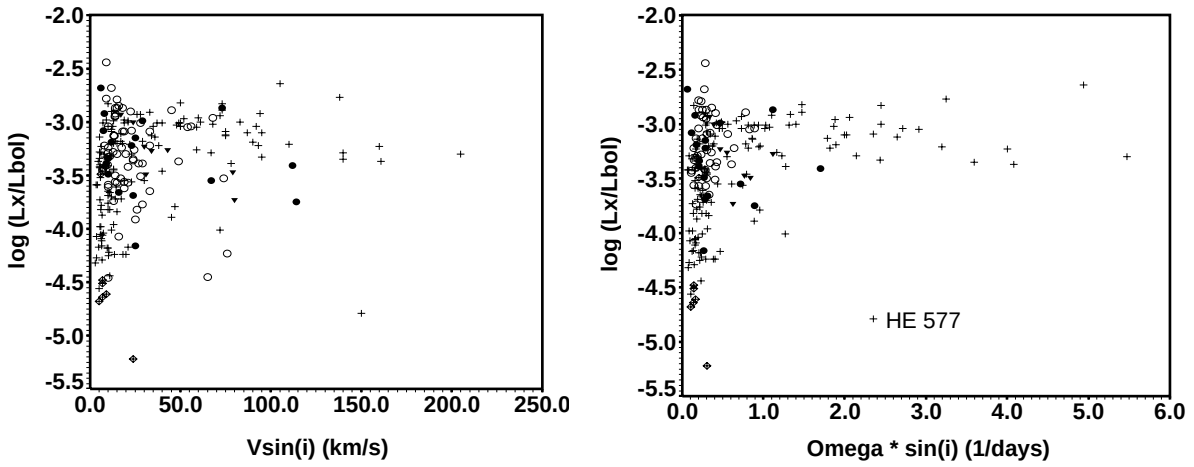

Fig. 7. Activity vs. rotation for Li-rich Taurus-Auriga stars (PMS: filled circles, ZAMS: filled triangles), and three comparison samples ('old' ZAMS stars (Hyades): diamond; 'young' ZAMS stars (IC 2602, α Per, IC 4665, Pleiades): crosses; CTTS/WTTS: open circles).

Pleiades, which are the two oldest clusters among the plotted samples. However, this might be a bias due to x-ray selection effects, as cluster membership is often determination on the basis of x-ray activity.

If we divide our Taurus sample into those stars we regard as ZAMS, and those we regard as PMS, we do not find a significant difference with respect to $\log(L_x/L_{bol})$. The mean values are -3.39 ± 0.10 for ZAMS stars and -3.35 ± 0.08 for PMS stars (the median is -3.34 for both). This is not very surprising, as many of the stars are apparently at – or close to – the saturation level.

7. Conclusions

Based on high-resolution echelle spectroscopy, we have shown that a large fraction of the ROSAT LRSs found in and around the Taurus-Auriga SFR (Wichmann et al. 1996), if placed at the distance of Taurus-Auriga, have three-dimensional motions consistent with those of previously known, bona-fide T Tauri stars in Taurus-Auriga. Furthermore, for many of them their $W_{\rm Li}$ indicates an age significantly lower than that of the Pleiades.

In all the SFR studied with ROSAT so far, a large, but varying fraction (always at least two thirds) of the ROSAT LRSs could be confirmed as truly young stars, i.e. having $W_{\rm Li}$ in excess of Pleiades stars (this fraction is much lower for the sample of stars south of Taurus studied by Magazzù et al. 1997, which is, however, farther outside a SFR than any of the other). While some of these young stars might pertain to the respective SFRs – especially those found close to molecular clouds –, it has been argued that many of them are part of a more dispersed population of young, low-mass Gould Belt stars (cf. Wichmann et al. 1997b, 1999).

The latter proposition was based on the perception that most nearby SFRs are not isolated entities, but are part of the kpc-size, young, expanding star forming complex known as the Gould Belt, and thus should be regarded as the presently most active parts of this structure, presumably embedded in a more dispersed distribution of young Gould Belt stars. This picture is supported by several pieces of evidence:

i) By investigating the spatial distribution of Li-rich low-mass stars around the Lupus SFR perpendicular to the galactic plane, Wichmann et al. (1997b) found that this distribution is peaked on the galactic latitude of the Gould Belt in this region, and drops off sharply towards the galactic plane.

ii) By cross-correlating the ROSAT All-Sky Survey (RASS) with the Tycho catalogue, Guillot et al. (1998b) found that the population of active, and hence presumably young, low-mass stars in the RASS is centered on a belt, whose best-fit parameter (like angular width, inclination with respect to the galactic plane, longitude of ascending node) are in perfect agreement with the Gould Belt. They also found that the distribution of these stars can be modeled best by assuming that they are distributed in a disk-like structure between the outer radius of the Gould Belt and some inner radius located about 120 pc inwards.

iii) Based on high-resolution echelle spectroscopy, Wichmann et al. (1999) found that nearly all of the Li-rich stars found near the Lupus SFR have lithium equivalent widths in excess of Pleiades stars, and hence are presumably significants younger, while the contamination with Pleiades-aged stars in this sample is only about 10 per cent, i.e. lower than in any other SFR studied so far.

For evaluating these facts, and placing our observations of Taurus-Auriga stars into the proper context, one should take into account that first, the sun is located within the Gould Belt, about half-way between its centre and its outer edge, and second, the Lupus SFR is located at the near edge of the Gould Belt, while Taurus-Auriga is located near the centre.

Thus, in the framework of the Gould Belt hypothesis, Lupus is the natural candidate for a very 'clean' sample of very young stars, as this is the direction where we look outwards from the Gould Belt's centre, towards its outermost and youngest parts. Moreover, due to the proximity of the outer edge in this direction, there is little chance to have much contamination.

On the other hand, Taurus-Auriga would appear as the natural candidate for a sample with a rather high degree of con-

tamination with relatively old stars. As we are looking towards the centre of the Gould Belt, i.e. its oldest parts, we expect that even Gould Belt stars in this region are rather old, nearly as old as the Gould Belt itself (i.e. about 60–80 Myrs). The far edge of the Gould Belt is more than 300 pc away, and thus outside the detection horizon of the RASS for typical x-ray luminosities of low-mass PMS stars (see the discussion in Guillot et al. 1998b).

Of course this raises the question of the origin of those stars in our sample that show large lithium equivalent widths, significantly in excess of Pleiades stars, i.e. those stars in our sample we classified as PMS stars. We cannot rule out, but we find it unlikely that these stars are part of a more diffuse Gould Belt background population, because such a population should be rather old already in this particular region, as discussed above. There is simply no natural candidate for a young PMS population other than the Taurus-Auriga SFR in this region.

We therefore argue that those ROSAT LRSs in Taurus-Auriga that could be confirmed as likely PMS stars in this work, might be directly related to the present Taurus-Auriga SFR. In fact, also Neuhäuser & Brandner 1998 report distances of 100–150 pc for the four ROSAT LRSs in Taurus observed by HIPPARCOS, in agreement with the distance of the Taurus-Auriga dark clouds.

Acknowledgements. This research has made use of the SIMBAD database, operated at CDS, Strasbourg, France. We express our thanks to the observers at the CfA telescopes, E. Bennett, P. Berlind, M. Calkins, J. Caruso, J. Degnan, A. Milone, J. Peters, R. Stefanik, and J. Zajac, and also to R. Davis for maintaining the CfA database of radial velocities. We also thank P. Corporon for carrying out some of the observations at OHP. RN acknowledges grants from the Deutsche Forschungsgemeinschaft (DFG Schwerpunktprogramm 'Physics of star formation'). We gratefully acknowledge the use of the Open Cluster Database, as provided by C.F. Prosser (deceased) and J.R. Stauffer, and which currently may be accessed at http://www-cfa.harvard.edu/∼stauffer/, or by anonymous ftp to cfa-ftp.harvard.edu (131.142.25.222), cd /pub/stauffer/clusters/. RW and JK acknowledge support by the German *Deutsche Forschungsgemeinschaft, DFG* project number KR 1053/5. CHFM acknowledges grants from CNPq proc. 200614/96-7 (NV). The ROSAT project is supported by the Max-Planck-Gesellschaft and Germany's federal government (BMBF/DLR).

References

Alexander D.R., Augason G.C., Johnson H.R., 1991, ApJ 345, 1014
Alcalá J.M., Krautter J., Schmitt J.H.M.M., et al., 1995, A&AS 114, 109
Alcalá J.M., Terranegra L., Wichmann R., et al., 1996, A&AS 119, 7
Baranne A., Queloz D., Mayor M., et al., 1996, A&AS 119, 373
Basri G., Martín E.L., Bertout C., 1991, A&A 252, 625
Bouvier J. 1990, AJ 99, 946
Bouvier J., Wichmann R., Grankin K., et al., 1997, A&A 318, 495
Canuto V.M., Mazzitelli I., 1991, ApJ 370, 295
Covino E., Alcalá J.M., Allain S., et al., 1997, A&A 328, 187
D'Antona F., Mazzitelli I., 1994, ApJS 90, 467
ESA, 1997, The Hipparcos and Tycho Catalogues, ESA SP-1200
Favata F., Barbera M., Micela G., Sciortino S., 1993, A&A 277, 428
Forestini M., 1994, A&A 285, 473
Frink S., Röser S., Neuhäuser R., Sterzik M.F., 1997, A&A 325, 613
Giampapa M.S., Prosser C.F., Fleming T.A., 1998, ApJ 501, 624
Gould B.A., 1879, in: Corni P.E. (ed.), Uranometria Argentina, Buenos Aires, p. 355
Guillout P., Sterzik M.F., Schmitt J.H.M.M., et al., 1998a, A&A 334, 540
Guillout P., Sterzik M.F., Schmitt J.H.M.M., Motch C., Neuhäuser R., 1998b, A&A 337, 113
Hauschildt P.H., Allard F., Baron E., 1998, ApJ, submitted
Hempelmann A., Schmitt J.H.M.M., Schultz M., Rüdiger G., Stępień K., 1995, A&A 294, 515
Høg E., Kuzmin A., Bastian U., et al., 1998, A&A 335, L65
Krautter J., Wichmann, R., Schmitt J.H.M.M., et al., 1997, A&AS 123, 329
Landolt A.U., 1983, AJ 88, 439
Magazzù A., Rebolo R., Pavlenko Y.V., 1992, ApJ 392, 159
Magazzù A., Martín E.L., Sterzik M.F., Neuhäuser R., Covino E., Alcalá J.M., 1997, A&AS 124, 449
Martín E.L., Rebolo R., Magazzù A., Pavlenko Y.V., 1994, A&A 282, 503
Neuhäuser R., Brandner W., 1998, A&A 330, L29
Neuhäuser R., Torres G., Sterzik M.F., Randich S., 1997 A&A 325, 647
Neuhäuser R., Sterzik M.F., Torres G., Martín E.L., 1995, A&A 299, L13
Prosser C.F., 1992, AJ 103, 488
Prosser C.F., Randich S., Stauffer J.R., Schmitt J.H.M.M., Simon T., 1996, AJ 112, 1570
Pöppel W., 1997, Fund. Cosmic Physics 18, 1
Randich S., Schmitt J.H.M.M., 1995, A&A 298, 115
Randich S., Schmitt J.H.M.M., Prosser C.F., Stauffer J.R., 1995, A&A 300, 134
Randich S., Schmitt J.H.M.M., Prosser C.F., Stauffer J.R., 1996, A&A 305, 785
Röser S., 1996, IAU Symp. 172, 481
Röser S., Bastian U., 1991, PPM Star Catalogue, Vols. I & II, Heidelberg: Spektrum Akademischer Verlag
Simon T., 1990, ApJ 359, L51
Soderblom D.R., Jones B.F., Balachandran S., et al., 1993, AJ 106, 1059
Stauffer J.R., Caillault J.-P., Gagné M., Prosser C.F., Hartmann L.W., 1994, ApJSS 91, 625
Stern R.A., Schmitt J.H.M.M., Kahabka P.T., 1995, Astrophys. J. 448, 683
Sterzik M.F., Durisen R.H., 1998, A&A 339, 95
Urban S.E., Corbin Th.E., Wycoff G.L., 1997, The ACT Reference Catalog, U.S. Naval Observatory, Washington, D.C.
Wielen R., 1997, A&A 325, 367
Wichmann, R., Krautter, J., Schmitt, J.H.M.M., et al., 1996, A&A 312, 439
Wichmann R., Krautter J., Covino E., et al., 1997, A&A 320, 185
Wichmann R., Sterzik M., Krautter J., Metanomski A., Voges W., 1997, A&A 326, 211
Wichmann R., Bastian U., Krautter J., Jankovics I., Rucinski S.M., 1998, MNRAS 301, L39
Wichmann R., Covino E., Alcalá J.M., et al., 1999, MNRAS 307, 909
Wuchterl G. 1999, in: Gimenez A., Guinan E.F., Montesinos B. (eds.), Stellar Structure: Theory and Test of Connective Energy Transport, ASP Conf. Series, Vol. 173. Astr. Soc. of the Pacific (San Francisco), p. 181